Formation and liquid permeability of dense colloidal cube packings

Sonja I. R. Castillo,* Dominique M. E. Thies-Weesie,† and Albert P. Philipse‡
Van 't Hoff Laboratory for Physical and Colloid Chemistry, Debye Institute for Nanomaterials Science, Utrecht University, Padualaan 8, 3584 CH Utrecht, The Netherlands
(Received 5 December 2014; published 26 February 2015)

The liquid permeability of dense random packings of cubic colloids with rounded corners is studied for solid hematite cubes and hollow microporous silica cubes. The permeabilities of these two types of packings are similar, confirming that the micropores in the silica shell of the hollow cubes do not contribute to the permeability. From the Brinkman screening length $\sqrt{k}$ of ∼16 nm, we infer that the relevant pores are indeed intercube pores. Furthermore, we relate the permeability to the volume fraction and specific solid volume of the cubes using the Kozeny-Carman relation. The Kozeny-Carman relation contains a constant that accounts for the topology and size distribution of the pores in the medium. The constant obtained from our study with aspherical particles is of the same order of magnitude as those from studies with spherical and ellipsoidal particles, which supports the notion that the Kozeny-Carman relation is applicable for any dense particle packing with (statistically) isotropic microstructures, irrespective of the particle shape.

DOI: 10.1103/PhysRevE.91.022311 PACS number(s): 82.70.Dd, 47.56.+r, 47.15.gp, 47.15.Rq

I. INTRODUCTION

Water through a sand bed, oil in a subsurface reservoir, and feed flow through filtration membranes are all examples of viscous flow through a porous medium [1–3]. Already in 1856, Darcy formulated an empirical relation between the permeated mass flow velocity U (in g/s) through a porous medium and the liquid permeability k of the medium [4,5]

$$U = k\frac{\rho_0}{\eta_0}\frac{\Delta P A}{L}, \tag{1}$$

with ρ_0 the solvent mass density, η_0 the solvent viscosity, ΔP the excess pressure applied over the medium, and A and L the cross-sectional area and the thickness of the medium, respectively. Later this empirical relation was derived theoretically from the Stokes equations for viscous flow [1,6,7].

In the case of porous media composed of densely packed particles, the liquid permeability k in Eq. (1) of such a packing can be connected to its porosity by the Kozeny-Carman (KC) relation

$$k = \frac{(1-\phi)^3}{C^+\phi^2}\nu^2, \tag{2}$$

where ϕ is the solid volume fraction of particles and C^+ a numerical constant determined by the topology and size distribution of the pores [5,7–10]. Here ν is defined as the specific solid volume of a particle

$$\nu = \frac{V_{\text{particle}}}{S_{\text{particle}}}, \tag{3}$$

with V_{particle} and S_{particle} the volume and the surface area of a particle, respectively. Although the KC relation was originally derived for a porous medium comprising capillary tubes, it was found to also predict the permeability of particle assemblies well and is therefore often employed in soil research and inorganic membrane technology [3,5,9,11–15]. Insight as to why the KC relation still holds despite the great variety in geometries can be gained by studying model systems, i.e., packings of particles with well-defined shape and size and known packing behavior [7,8,16–19]. Studies on (binary) hard spheres have demonstrated that the KC relation is adequate for ordered as well as random dense packings [7,8,18]. From these studies, it can be deduced that the main requirements for the KC relation to apply are that the packing is sufficiently dense and (statistically) isotropic [7,8]. These main requirements were also deduced from experimental and numerical studies with aspherical particles such as spiky particles [16] and ellipsoids [19]. The studies indicate that C^+ is quite insensitive to the particle shape.

In this work, we investigate the liquid permeability of packings of nonspheres in the form of cubes. In doing this, we benefit from the shape and size control in recently developed synthesis methods for micron-sized colloidal cubes [20,21]. The aspherical colloids used in our experiments actually have a superball shape, i.e., cubic with rounded corners (Fig. 1). Particles with this cubic shape have gained interest in the past due to the remarkable packing behavior arising from the rounded corners, in both experimental and computational studies [20,22–30]. The volume fraction these colloidal cubes can achieve when packed randomly is ∼0.74, which is markedly higher than for randomly packed spheres (∼0.64) or even ellipsoids (∼0.71) [28,31,32]. In addition to the packing behavior, the superball shape affects the particle volume and particle surface area. Therefore, in order to arrive at a correct expression for the specific solid volume ν and consequently at a correct permeability via Eq. (2), we derive mathematical expressions for the superball volume and surface area (see Appendix B).

The cubic colloids we use in this research are about 1 μm in edge length and are composed of hematite (α-Fe_2O_3). From these hematite cubes, hollow microporous silica cubes (pore diameter <2 nm [33]) can be prepared by first growing a shell of microporous silica around the hematite core and subsequently dissolving the core [20,21,34]. In this work,

*s.i.r.castillo@uu.nl
†d.m.e.thies-weesie@uu.nl
‡a.p.philipse@uu.nl

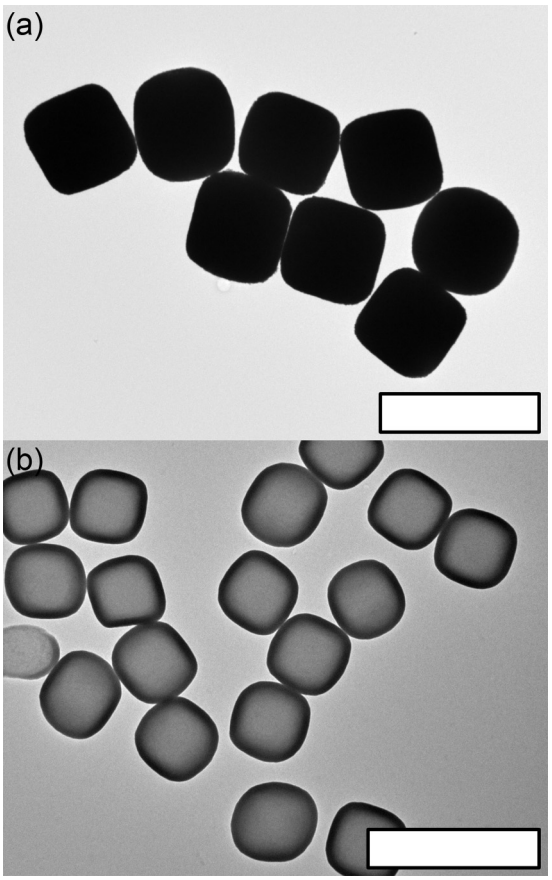

FIG. 1. Representative TEM images of the cubic colloids used for the packing formation and permeation experiments: (a) solid hematite cubes without silica coating (1477 nm) and (b) hollow microporous silica cubes (940 nm). The scale bars represent 2 μm.

both the solid hematite cubes and hollow silica cubes are applied for cube packings. The advantage of these large cubes over nanosized cubes is that they can overcome the surface roughness and porosity of a substrate more easily. Consequently, they can be conveniently applied in permeation experiments using a permeable filter substrate.

This paper is organized as follows. First, we discuss the experimental setup used for the cube packing formation and the permeation experiments. Second, we present the results of these experiments and calculate the permeabilities of the formed packings as a function of the amount of cubes using Darcy's law (1). Subsequently, we calculate the C^+ value by correlating the found permeabilities to the Kozeny-Carman relation in Eq. (2).

II. EXPERIMENT

A. Cubic colloids

For the permeation experiments, two different types of cubic colloids were applied: solid hematite cubes and hollow microporous silica cubes (Fig. 1). In the case of the solid cubes, liquid can only flow alongside the particles, whereas for the hollow cubes liquid can also flow through the particles using the micropores. The cubes were synthesized following the procedures described in Refs. [20,21,34] and were dispersed in Millipore water. Table I shows their average edge length and size polydispersity.

TABLE I. Specifications of the applied cubic colloids regarding their average edge length (size), size polydispersity (pd%), silica shell thickness, m value, and semiaxis aspect ratio (a/b).

Cubes	Size (nm)	pd% (%)	Silica shell (nm)	m value	a/b
Solid hematite	1477	4		3.8	0.99
Hollow silica	940	3	50	3.1	1.00

In short, the hematite cubic colloids were synthesized by aging a highly condensed mixture of aqueous solutions of iron chloride [2.0M, iron(III) chloride hexahydrate, p.a., Sigma-Aldrich] and sodium hydroxide (5.4M, p.a., Emsure) at 100 °C for eight days. Subsequently, the resulting sol was washed by centrifugation and redispersion in Millipore water until pH ~ 7 was reached. For the synthesis of the hollow microporous cubes, 2.4 g (dry weight) of hematite cubic seed particles were first dispersed in 110 mL of aqueous solution of polyvinylpyrrolidone [90 g/L, 40 kg/mol polyvinylpyrrolidone (PVP), Aldrich] and stirred overnight to let the PVP adsorb effectively onto the hematite cubes. Afterward, the excess of PVP was washed away and the cubes were redispersed in ethanol (100%, Interchema). A smooth and uniform silica coating was then grown onto the PVP-functionalized hematite cubes by slowly adding the silica precursor tetraethoxysilane (10 mL of tetraethoxysilane in 10 mL ethanol, purum, Fluka) in a mixture of ethanol and Millipore water. The reaction was catalyzed by the base tetramethylammonium hydroxide (25% in water, Fluka). The entire reaction was conducted under mechanical stirring and ultrasonication at a constant temperature of 20 °C to prevent aggregation of the particles during synthesis. Finally, the hematite core was dissolved using hydrochloric acid (6M, Merck). Since the silica coating is porous, the acid can access the hematite core and the ions from the dissolved hematite can diffuse away to the surrounding water. The hollow cubes were then washed by centrifugation and redispersion in ethanol until pH 6–7 was reached.

Since these cubic colloids are not perfectly cubic but have rounded corners, their shape is best described by a superball [30]

$$\left|\frac{x}{r}\right|^m + \left|\frac{y}{r}\right|^m + \left|\frac{z}{r}\right|^m \leqslant 1, \tag{4}$$

where r is the particle radius and m the deformation parameter. For a sphere, $m = 2$ and the particle radius is the sphere radius, while for a perfect cube, m approaches infinity and the particle radius is half the edge length (Fig. 2). Between these two m values, the shape of the particle resembles that of a cube with rounded corners [Fig. 2(a)]. The particle radius of exemplary superball shapes between $m = 2$ and $m \to \infty$ is indicated in Fig. 2(b).

We cannot simply assume a perfect cubic shape for these colloids because their superball shape influences the packing behavior, particle volume, and particle surface area. These parameters should be known in order to analyze the liquid permeability of cube packings correctly. The m values for the applied cubes were determined by examining the shape of

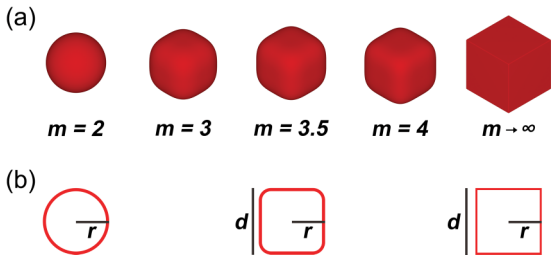

FIG. 2. (Color online) The colloidal cubes in this study have a superball shape of which the precise shape depends on the deformation parameter m. (a) The shape changes from a sphere ($m = 2$) via cubes with rounded corners to a perfect cube ($m \to \infty$). (b) Cross-sectional views of superballs at given m values indicating the particle radius r; $d = 2r$ with d the edge length of a cube.

an ensemble of cubes using transmission electron microscopy (TEM) images of single cubes. Because the TEM images give a two-dimensional projection of the particles, the circumference of the cubes was fitted with

$$\left|\frac{x}{a}\right|^m + \left|\frac{y}{b}\right|^m = 1, \tag{5}$$

with a and b the semiaxes of a particle. Ideally, for a cube $a = b = r$, but the semiaxes are explicitly defined to take into account the deviations from the ideal edge length ratios of the colloidal cubes [35]. The TEM images can be fitted quite precisely to Eq. (5). The average m values and the aspect ratios of the semiaxes a/b for the used cubes are listed in Table I.

B. Packing formation and permeation experiments

To determine the liquid permeability of an assembly of cubic colloids, first a packing of cubes was formed by forced convection onto a permeable Millipore polymeric filter (VCWP02500, pore diameter equal to 0.1 μm) as the substrate. The used setup is schematically depicted in Fig. 3 and consists of a glass solvent reservoir (II), which is attached to a nitrogen gas source (I) and a glass dispersion cell (III). The cylindrical dispersion cell (length 21 cm, inner diameter 1.9 cm, and approximate volume 67 mL) contains the aqueous dispersion of particles and, at the bottom, the Millipore filter supported by a metallic grid. The solvent (Millipore water from Synergy Purification Systems) can flow through the setup by opening the valves (vI and vII) and by applying an excess pressure ΔP using nitrogen gas. The pressure of the nitrogen gas is controlled and measured accurately. The permeated water is collected in a beaker (IV) and its mass is measured throughout the experiment with a balance (V). The constant excess pressure forces the particles in the dispersion cell down, packing them onto the Millipore filter.

Once a packing was formed, its permeability was determined with the same setup by flowing water through the packing at increasing excess pressure. For a typical experiment, approximately 100 mL of Millipore water was flowed through. The mass of the permeated water was measured as a function of time. The permeation experiments were repeated at least three times at the same conditions and a fit was made through the data points of all measurements.

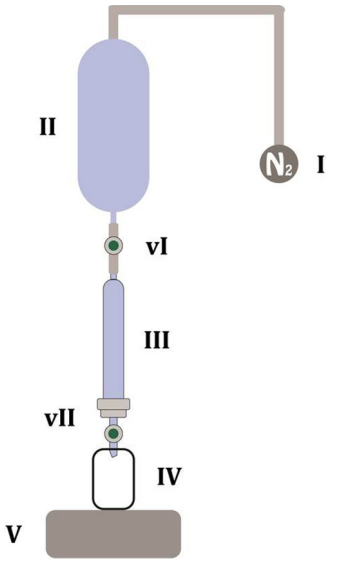

FIG. 3. (Color online) Schematic image of the setup used for packing formation and permeation experiments. A nitrogen gas source (I) is connected to a glass solvent reservoir (II). The solvent enters the glass dispersion cell (III) via valve vI. The cubic colloids inside the dispersion cell are forced down by the excess pressure exerted by the solvent and packed onto the Millipore filter at the bottom of the dispersion cell. The solvent passes through the packing and Millipore filter via valve vII and is collected in a beaker (IV). The permeated solvent mass is accurately recorded by a balance (V).

C. Characterization

After all permeation measurements were conducted, the dispersion cell was emptied and the packing was dried in open air. The morphology of the packings was examined with a scanning electron microscope (FEI XL30 FEG) operated at 5 kV. The dry packings were stuck to a stub using a conductive carbon sticker and were then coated with a layer of platinum of typically 6 nm prior to analysis.

III. RESULTS AND DISCUSSION

A. Packing formation

The formation of a packing is visible in the plot of the permeated solvent mass as a function of time. Figure 4(a) shows a typical plot measured during the formation of a packing. Unlike for flow through a packing of constant thickness, the permeated mass through a growing packing does not grow linearly in time due to the increase of the hydrodynamic friction during packing formation [7,19,36]. From the derivation described in Appendix A, it follows that for a growing, incompressible and homogeneous packing, the permeated solvent mass W scales with the square root of the time t rather than with t according to

$$\frac{W}{\sqrt{\Delta P}} \propto \sqrt{t}, \tag{6}$$

where ΔP is the applied excess pressure [7,19,36]. Notably, the data plotted in Fig. 4(a) do not follow the $\sqrt{t}$-scaling relation of Eq. (6) throughout the process of packing formation. The fit of $W \propto \sqrt{t}$ displayed in Fig. 4(a) illustrates that

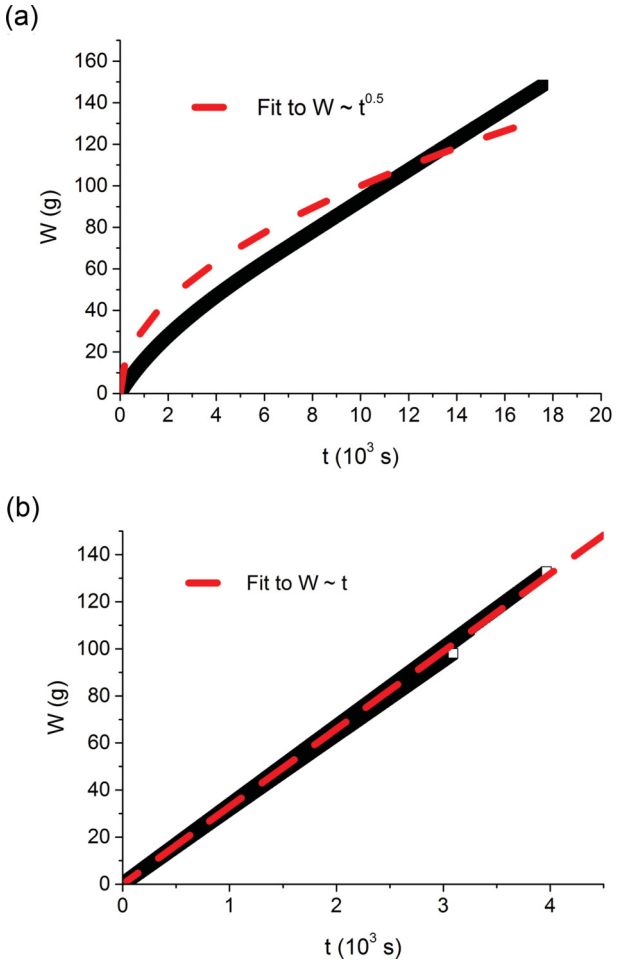

FIG. 4. (Color online) Typical plots of the permeated solvent mass W as a function of time, measured during packing formation and permeation experiments. (a) During packing formation, the permeated mass deviates from the $\sqrt{t}$-scaling relation of Eq. (6) (dashed line) due to settling of the cubes. (b) During permeation experiments, the permeated mass grows linearly in time with a mass flow velocity of U, which is equal to the slope of the linear fit shown with the dashed line. From the constant slope it can be inferred that the microstructure of the packing does not change in time.

the actual permeated solvent mass is consistently lower than expected from Eq. (6). This result suggests that the packing is thicker than expected from packing formation by forced convection only. The deviation from the $\sqrt{t}$-scaling relation has previously been related to the settling of the particles during packing formation [36]. Indeed, settling of both solid and hollow cubes is a process that occurs during packing formation, owing to their short gravitational lengths (approximately 24 nm for the solid cubes and 890 nm for the hollow cubes). Once all cubes have been packed, the permeated mass grows linearly in time [Fig. 4(b)], as expected.

The dried packings [representative images shown in Figs. 5(a) and 5(b)] were analyzed with scanning electron microscopy (SEM) to investigate the structure of the packings. We assume that the pore structures of dried packings correspond to those of packings during the permeation measurements. For SEM analysis, the packings were broken into pieces and placed onto a SEM stub [Fig. 5(c)]. However, the

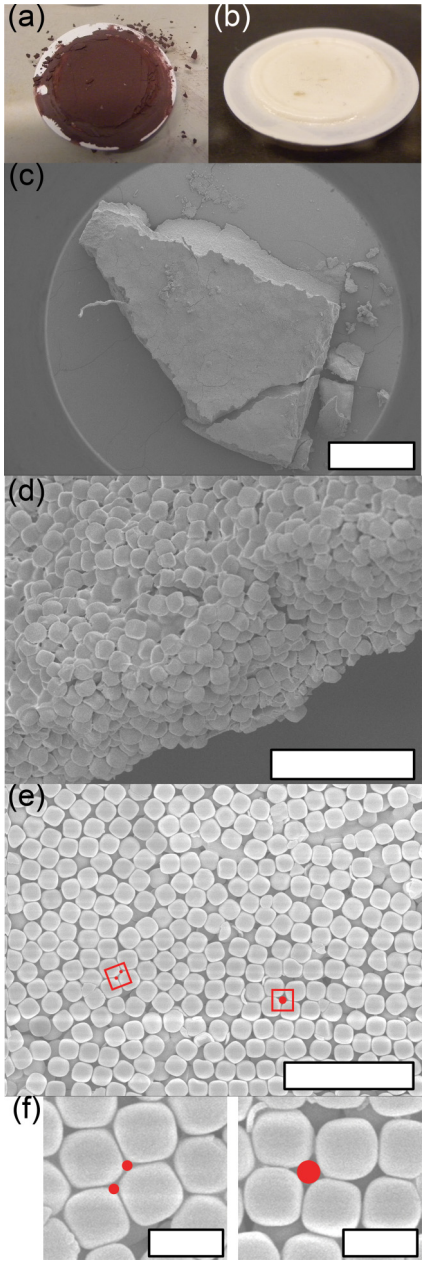

FIG. 5. (Color online) Representative images at increasing magnification of packings after drying. Photos of dry packings of (a) solid hematite cubes and (b) hollow silica cubes. The white disk underneath each packing is the Millipore filter substrate with a diameter of 2.5 cm. (c) The packings were broken into pieces to analyze them with SEM. The scale bar represents 500 μm. (d) The solid hematite cubes are disordered within a layer. Scale bar is 10 μm. (e) High-magnification SEM image of the upper layers of a dry packing. The tilted square (left) indicates a shifted squarelike arrangement of cubes. The square (right) indicates a squarelike arrangement of cubes. The resulting pores are marked by the red circles. The scale bar is 5 μm. (f) Magnifications of the arrangements and resulting pores indicated in (e). Pore diameters are ~180 nm (left) and ~300 nm (right). Scale bars represent 1 μm.

packings were very fragile and brittle, which hampered easy handling: As soon as a dried packing was touched, it fell apart into a powder.

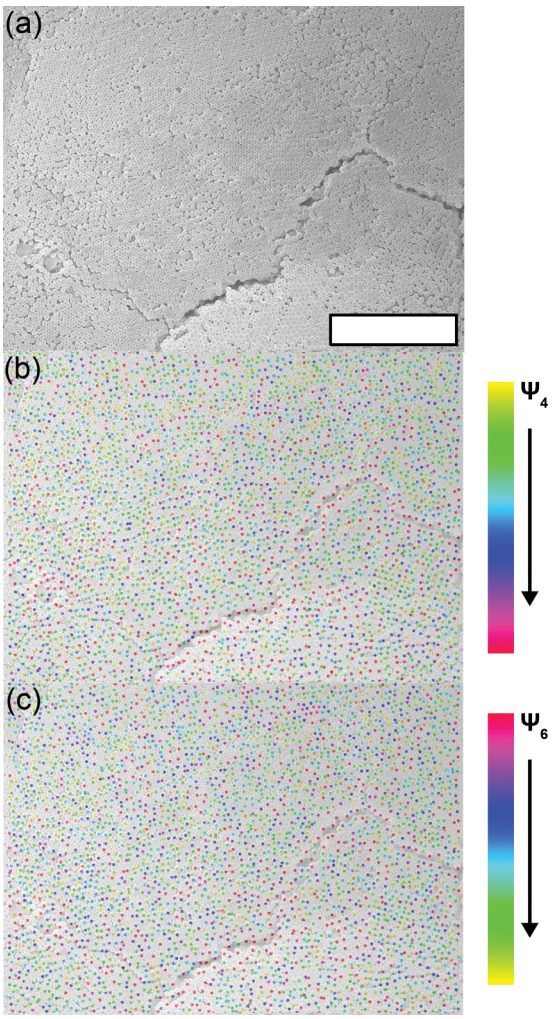

FIG. 6. (Color online) (a) Typical SEM image of the visible top layer of the bottom of a packing formed by hollow silica cubes. The cracks were created during drying and were not present during the permeation measurements. The scale bar represents 20 μm. (b) Ψ_4 analysis of the packing in (a). The colors of the dots indicate the extent of cubic ordering, where yellow to green signifies high cubic ordering and red to purple low cubic ordering. (c) Ψ_6 analysis of the packing in (a). The colors of the dots indicate the extent of hexagonal ordering, where red to purple signifies high hexagonal ordering and yellow to green low hexagonal ordering. Clearly there is significant short-range cubic as well as hexagonal order within a layer.

The packings were formed from many layers of densely packed cubes, but because SEM only allows visualization of the surface of a packing, we could only analyze the cubes in the visible upper layer or from the side. Typical SEM images of solid cubes packings are displayed in Fig. 5. For the packing in Fig. 5(d), it seems that the cubes are disordered. However, regions that exhibit some ordering are also observed [Fig. 5(e)]. The observed disorder could have been caused by the fast settling of the solid cubes, as well as by the brittleness of the dry packings. The packings of the hollow silica cubes also show signs of ordering, though not of long range. The SEM image in Fig. 6(a) shows the bottom of a packing, clearly displaying the difference from the top of a packing. The Ψ_4 and Ψ_6 analyses of the visible layer in Fig. 6(a) signify the extent of cubic (Ψ_4) or hexagonal (Ψ_6) ordering [37,38]. From Figs. 6(b) and 6(c) it is clear that both cubic and hexagonal segments are present, but only in a short range within a layer: Cubic ordering is indicated with green in Fig. 6(b) and hexagonal ordering is indicated with red to purple in Fig. 6(c). We believe that the packings did not contain large cracks that channel the Millipore water directly through the packing with little resistance. The cracks seen in Fig. 6 most probably emerged during the drying of the packing and were not present during the measurements.

TABLE II. Properties of packings composed of solid hematite cubes and hollow silica cubes with regard to the dry weight of used cubes m_{cubes}, the mass flow velocity over the applied excess pressure U_{m}, the calculated liquid permeability k [Eq. (7)], the Brinkman screening length $\sqrt{k}$, and the calculated constant C^+ [Eq. (2)].

Cubes	m_{cubes} (g)	U_{m} (kg/s Pa)	k (nm^2)	$\sqrt{k}$ (nm)	C^+
Solid hematite	0.19	5.6×10^{-10}	256	16	8.1
	0.39	3.3×10^{-10}	306	17	6.8
	0.72	1.3×10^{-10}	225	15	9.2
Hollow silica	0.12	3.2×10^{-10}	223	15	10.7
	0.23	2.2×10^{-10}	298	17	8.0
	0.41	1.1×10^{-10}	273	17	8.7

B. Permeation experiments

The liquid permeability of the formed packings at different excess pressures was investigated by flowing Millipore water through the packings. This procedure was repeated at least three times for each pressure, after which the data points were fitted to yield a plot as shown in Fig. 4(b). The applied pressure remained constant during the measurement, as well as between each repeated measurement. From the linear increase of the permeated mass in time shown in Fig. 4(b), we infer the presence of Darcian flow as described by Eq. (1). The slope of the permeation plot is the mass flow velocity U and since the mass flow velocity hardly changes in time, we can conclude that the packing microstructure does not change in time either.

Figure 7 shows the mass flow velocity U measured at different excess pressures and amount of cubes, i.e., packing thickness, for both the solid hematite cubes and hollow silica cubes. As expected, the mass flow velocity increases for higher pressures and decreases for larger amount of cubes. The slope of these plots is the mass flow velocity over the excess pressure, defined as U_{m} ($U_{\text{m}} = U/\Delta P$). Evidently, U_{m} decreases with increasing amount of cubes (Table II).

C. Permeability calculations

As described in the Introduction, we can calculate the permeability of a cube packing using Darcy's law. Subsequently, the permeability is related to the packing porosity, i.e., the particle volume fraction ϕ in the packing, from which we can determine the C^+ value in the Kozeny-Carman relation to assess whether or not C^+ is affected by the cube shape.

1. Permeability from Darcy's law

From the permeation experiments, we obtain the mass flow velocity over the excess pressure U_{m} (Fig. 7), with which we

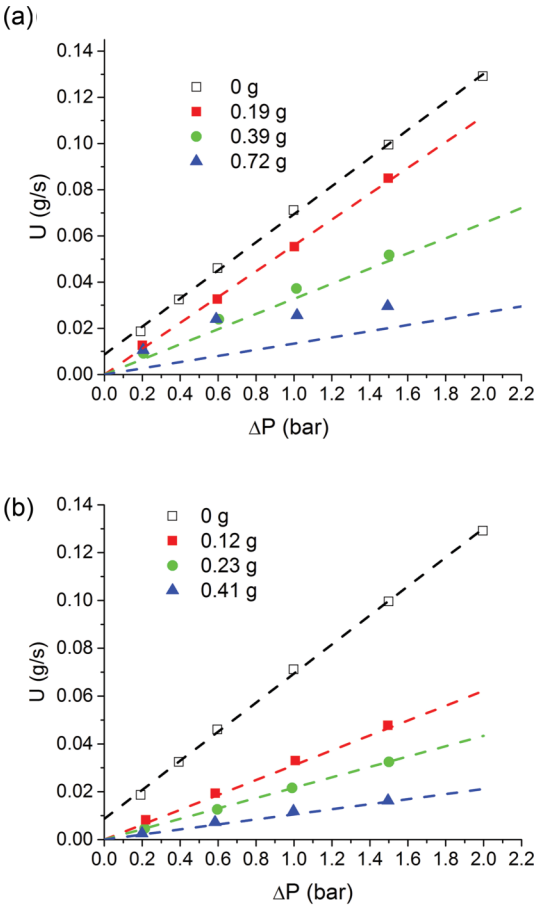

FIG. 7. (Color online) Mass flow velocities U as a function of the applied pressure ΔP for packings of (a) solid hematite cubes and (b) hollow silica cubes. The mass flow velocity increases with increasing ΔP and decreasing amount of cubes. The drawn lines are linear fits through the data points and their slope is U_m ($U_m = U/\Delta P$) as listed in Table II.

can calculate the liquid permeability k of the packing using Eq. (1):

$$k = \frac{4\eta_0 L U_m}{\pi D^2 \rho_0}, \tag{7}$$

with η_0 the solvent viscosity, D the diameter of the packing, ρ_0 the solvent mass density, and L the packing thickness. Since the values for the first three quantities are set for our experiments ($\eta_0 = 0.89$ mPa s, $D = 0.019$ m, and $\rho_0 = 1000$ kg/m^3), only L and U_m vary.

The mass flow velocity over the excess pressure U_m was determined from the permeation experiments and the values for each packing are listed in Table II. However, the packing thickness L could hardly be determined accurately due to the fragility of the dry packings. Therefore, we used predetermined particle volume fractions ϕ instead. The volume fraction is related to the packing thickness L as follows:

$$\phi = \frac{V_{cubes}}{V_{packing}} = \frac{4V_{cubes}}{\pi D^2 L} = \frac{4V_{cube} m_{cubes}}{\pi D^2 L m_{cube}}, \tag{8}$$

with V_{cubes} the total volume of all cubes used to form the packing, $V_{packing}$ the volume of the resulting packing, V_{cube} the volume of a single cube, m_{cubes} the dry weight of cubes used to form the packing, and m_{cube} the mass of a single cube. For $V_{packing}$, we assume a cylindrical packing with height L and diameter D, which corresponds to the packing diameter D used in Eq. (7). To calculate V_{cube}, we used the expression for the volume of a superball given in Appendix B [Eq. (B11)]. This expression depends on the precise m value of the cubes and shows that a cube with edge length 1000 nm has a volume of approximately $V_{cube} = 7.3 \times 10^{-19}$ m^3 for $m = 3.1$, $V_{cube} = 7.9 \times 10^{-19}$ m^3 for $m = 3.8$, and $V_{cube} = 1.0 \times 10^{-18}$ m^3 for $m \to \infty$. The mass of a single solid hematite cube and the mass of a single hollow silica cube are $m_{cube,solid} = V_{cube}\rho_{hematite}$ ($\rho_{hematite} = 5.25$ g/cm^3) and $m_{cube,hollow} = V_{silica\ shell}\rho_{silica}$ ($\rho_{silica} = 2$ g/cm^3), respectively. Combining Eqs. (7) and (8) leads to the following expression for the liquid permeability of a cube packing dependent on the volume fraction of cubes:

$$k = \frac{16\eta_0}{\pi^2 D^4 \rho_0} \frac{U_m V_{cubes}}{\phi} = \frac{16\eta_0}{\pi^2 D^4 \rho_0} \frac{U_m V_{cube} m_{cubes}}{\phi m_{cube}}. \tag{9}$$

The permeabilities listed in Table II are the averages of permeabilities calculated for volume fractions between 0.65 and 0.74 for the solid cubes and between 0.65 and 0.71 for the hollow cubes, where we assume that the occurrence of each volume fraction is equally probable. These volume fraction ranges correspond to dense assemblies of randomly packed superballs with the m values of the cubic particles used, $m = 3.8$ and 3.1, respectively [27,28,39]. At the highest volume fraction, the cubes form maximally random jammed packings [28]. These volume fraction ranges are realistic, since the SEM images of the packings in Figs. 5 and 6 show dense assemblies without long-range order.

Clearly, the calculated permeabilities are scattered around an average value of 262 nm^2 ± 17 nm^2 for the solid hematite cubes and 264 nm^2 ± 12 nm^2 for the hollow silica cubes. Because the liquid permeabilities of both packings do not differ significantly, we infer that the porosity of the microporous silica shell of the hollow cubes does not play a significant role in the permeation properties of the packings formed in these experiments. Therefore, flow through the packing does not affect any processes, e.g., catalysis reactions [40], that may occur inside the hollow cubes; penetration of a substance into a hollow cube is diffusion controlled, regardless of liquid flowing through the cube packing.

That liquid flow primarily occurs through intercube pores also follows from the Brinkman screening length $\sqrt{k}$, which is a measure for the viscous decay of a disturbance produced in a liquid [8,41,42]. For a liquid flowing through a porous medium composed of particles, hydrodynamic screening is caused by adjacent particles and therefore the Brinkman screening length is an indication of pore sizes that conduct the liquid. The Brinkman screening lengths given in Table II lie for all packings around 16 nm. Filtration experiments with aqueous dispersions of small silica spheres (Ludox TMA, Sigma-Aldrich) with a diameter of approximately 16 nm show that these small silica spheres can indeed pass through the cube packings. However, their mass flow velocity is considerably lower than that of pure Millipore water, $U = 7.8 \times 10^{-5}$ and 7.2×10^{-3} g/s at $\Delta P = 0.6$ bar, respectively. Admittedly, cake formation of small silica spheres on top of the cubes

packing could have contributed to the decreased flow velocity. Nevertheless, the low mass flow velocity reveals that the silica spheres cannot pass through easily and that the pores of the packing are not much larger than the silica spheres. We also verified that dye molecules, on the other hand, have a permeation velocity similar to that of Millipore water, signifying that they easily permeate a cube packing.

The typical pore size derived from the Brinkman screening length is much smaller than the pores created when four cubes are arranged in a squarelike or shifted squarelike arrangement. Analysis on high-magnification SEM images of cubes packings shows that in the former case, a pore of approximately 300 nm in diameter is created while in the latter case, a pore of ~180 nm in diameter is formed. In Figs. 5(e) and 5(f), the two arrangements and the corresponding pores are indicated. Consequently, from solely the SEM images of the packings, a larger permeability of the packings is expected compared to the permeabilities measured in our experiments. This difference illustrates that a three-dimensional cube packing is composed of two-dimensional cube layers that are randomly shifted with respect to each other such that the large pores in the two-dimensional layers are blocked by cubes from other layers, resulting in effectively smaller pores.

2. *Permeability from the Kozeny-Carman relation*

To determine C^+ following Eq. (2), we only require ν^2, the specific solid volume squared of the cubes used. An expression for the volume of a superball dependent on the m value has been reported previously by Torquato and co-workers [29,30], to which our expression (B11) corresponds. However, an expression for the surface area of a superball is lacking. Our derivation and numerical calculations of the volume and surface area of superballs from $m = 2$ to $m \to \infty$ are given in Appendix B. These calculations show that the specific solid volume for a sphere ($m = 2$) and a perfect cube ($m \to \infty$) both equal $\nu = \frac{1}{3}r$ and that ν^2 increases between $m = 2$ and 5 (Fig. 8). For the cubes used in this study with $m = 3.8$ and 3.1, $\nu^2 = 3.4 \times 10^{-14}$ and 3.3×10^{-14} m^2, respectively.

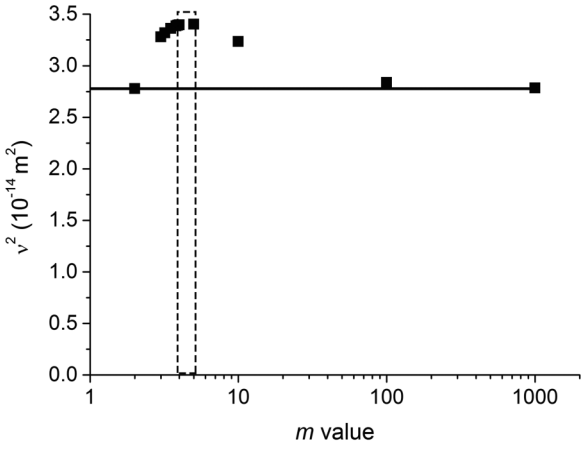

FIG. 8. The specific volume squared ν^2 is equal to $(\frac{1}{3}r)^2$ in the case of a sphere ($m = 2$) and a perfect cube ($m \to \infty$), as indicated by the drawn solid line. For m values between $m = 2$ and 5, ν^2 increases. In these calculations, $r = 500$ nm, corresponding to an edge length of 1000 nm. The dashed lines mark the range of m values of the cubes used in the experiments.

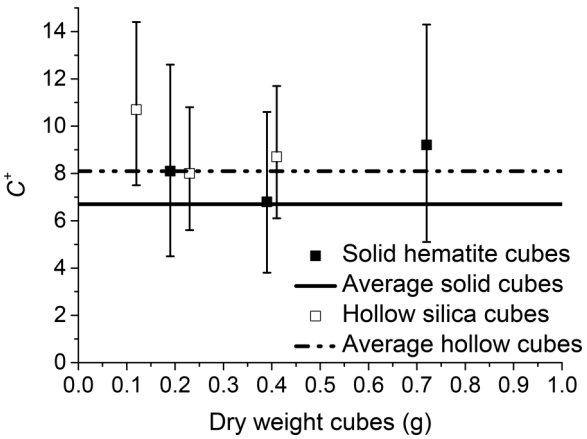

FIG. 9. The C^+ values calculated by the Kozeny-Carman relation (2) for the solid and hollow cubes. The values are scattered around $C^+ = 8.1$ and 9.1 for solid and hollow cubes, respectively.

Finally, Fig. 9 shows the values for C^+ for each packing. The error bars correspond to the dependence of the C^+ value on the assumed volume fraction: The highest value assumes the lowest volume fraction, whereas the lowest value assumes the highest volume fraction. For the solid hematite cubes, the C^+ value averages around 8.1, while for the hollow silica cubes the average C^+ value is 9.1 The rather consistent value of C^+ confirms that the permeability of the cube packings can be described by the Kozeny-Carman relation. Moreover, the found values of C^+ for cube packings are comparable to those found for (binary) hard spheres and ellipsoids [7,8,19], which supports the notion that the essential requirement for the Kozeny-Carman relation is that the investigated packing has a dense and (statistically) isotropic microstructure. Apparently, in dense particle packings, the shape of the particles is of minor importance: The permeated liquid cannot identify the shape of the particles because the decay length $\sqrt{k}$ of the hydrodynamic disturbance is much smaller than the particle size.

IV. CONCLUSIONS AND OUTLOOK

Dense cube packings can be formed by forced convection, leading to randomly packed cubic colloids. The liquid permeability k of these dense random packings follows Darcy's law as well as the Kozeny-Carman relation. Packings of solid and hollow cubes have very similar permeabilities, showing that the micropores of the hollow silica cubes do not contribute to the permeability of the packing. Instead, the resulting packings have an indicative pore size $\sqrt{k}$ (the Brinkman screening length) of 16 nm. From the KC relation, average C^+ values of 8.1 and 9.1 are found for solid and hollow cubes packings, respectively. Since the found C^+ values are comparable to those previously observed for packings of (binary) hard spheres and ellipsoids, we conclude that the KC relation is indeed generally applicable for dense packings with (statistically) isotropic microstructure and is insensitive to particle shape: Viscous dissipation by the total particle surface in a given particle packing volume is hardly affected by the geometrical details of this surface.

For future experiments, efforts could be put into creating cube packings with long-range order, which lead to higher

volume fractions (0.87 for $m = 4$) [27–29]. Packing the cubes in an ordered fashion also enlarges the amount of nearest neighbors from approximately 8 to 12 [27–29]. Since the permeability of a packing is lower for a larger number of nearest neighbors [8,18], an ordered cube packing would very likely lead to a decreased pore size. One method to achieve long-range order is by adding nonadsorbing depletants to the dispersion, which cause the cubes to form well ordered packings, as described by Rossi *et al.* [20]. Forced sedimentation of these well ordered arrays onto the Millipore filter substrate would then lead to packings containing these well ordered assemblies.

ACKNOWLEDGMENTS

The authors are grateful to Peter de Graaf, Matthijs Krijnen, Hans Heesen, Stephan Zevenhuizen, and Bonny Kuipers for constructing the experimental setup and corresponding measurement program. Dr. Rob Koelman is thanked for the mathematical derivations of the volume and surface area of superballs. The authors thank Dr. Laura Rossi for providing the algorithm to fit the m values and Dr. Jan Hilhorst and Vera Meester are thanked for their help on the IDL program for Ψ_4 and Ψ_6 analysis. Álvaro González García is acknowledged for making the schematic images of superballs. This research was supported by the Dutch Technology Foundation STW, Netherlands under the partnership program STW-Hyflux CEPAration Inorganic and Hybrid Membranes Project No. 11020.

APPENDIX A: DERIVATION OF THE $\sqrt{t}$-SCALING RELATION

To derive the $\sqrt{t}$-scaling relation for growing packings in the experiments described in this study, we briefly review the derivation reported in Ref. [36]. We consider the situation as depicted in Fig. 10. Here the cylindrical cell represents the dispersion cell used in the experiments with a substrate at the bottom upon which the particles assemble as the valve is opened (Fig. 3). The cell is initially filled up to height H with a dispersion containing a particle volume fraction ϕ_d. When the valve is opened, the solvent flows away, the dispersion level decreases by $h(t)$, and a homogeneous and incompressible packing of thickness $L(t)$ is formed. The particle volume fraction of the packing is given by ϕ_p.

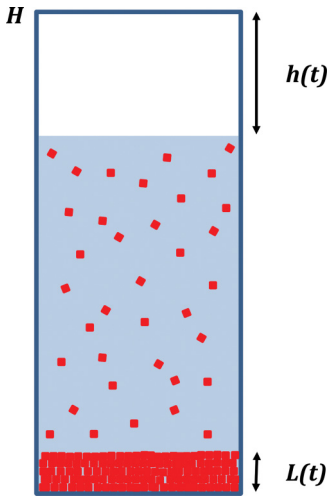

FIG. 10. (Color online) Schematic illustration of the dispersion cell during packing formation. Initially, the cell is filled to height H with dispersion with particle volume fraction ϕ_d. During packing formation, the liquid level decreases by $h(t)$ and a packing of thickness $L(t)$ and particle volume fraction ϕ_p is formed.

The initial total volume of particles is $H\phi_d$, which should equal the total particle volume at time t after opening the valves. Therefore, the following equality holds, from which the packing thickness $L(t)$ as a function of time can be deduced:

$$H\phi_d = L(t)\phi_p + \phi_d(H - L(t) - h(t)), \tag{A1}$$

$$L(t) = h(t)\,\frac{\phi_d}{\phi_p - \phi_d}. \tag{A2}$$

By combining Eq. (A2) and Darcy's law, we can relate the applied excess pressure ΔP, solvent viscosity η_0, solvent mass density ρ_0, and liquid permeability k to the thickness of a growing packing

$$U = \frac{dh(t)}{dt} = \frac{k\rho_0}{\eta_0}\,\frac{\Delta P A}{L(t)}. \tag{A3}$$

Substitution of Eq. (A2) in Eq. (A3) yields a differential equation in $h(t)$, which has the solution

$$h^2(t) = \frac{2k\Delta P}{\eta}\,\frac{(\phi_p - \phi_d)}{\phi_d}\,t. \tag{A4}$$

Since $h(t)$ is proportional to the mass of permeated solvent W, we arrive at the $\sqrt{t}$-scaling relation

$$\frac{W}{\sqrt{\Delta P}} \propto \sqrt{t}. \tag{A5}$$

If the packing is not growing in time, which is the case in the permeation experiments, L is a constant and Eq. (A3) simply reduces to

$$h(t) = \frac{k}{\eta}\,\frac{\Delta P}{L}\,t. \tag{A6}$$

Therefore, the permeated mass increases linearly in time.

APPENDIX B: SUPERBALL

The shape of the cubic particles is best described by the shape of a superball

$$\left|\frac{x}{r}\right|^m + \left|\frac{y}{r}\right|^m + \left|\frac{z}{r}\right|^m \leqslant 1, \tag{B1}$$

with which one can interpolate between octahedral-like shapes and cubiclike shapes with radius r, depending on the deformation parameter m. For a sphere and a perfect cube, $m = 2$ and $m \to \infty$, respectively. The particle shape and corresponding particle radius for exemplary superball shapes between $m = 2$ and $m \to \infty$ are indicated in Fig. 2(b). For the synthesized cubic particles, m lies between 3 and 4. In the following sections, we will derive expressions for the volume and the surface area of a superball with deformation parameter m and radius $r = 1$, using this parametric representation of an octant

of a superball

$$x = t^{1/m} s^{1/m},$$
$$y = (1-t)^{1/m} s^{1/m}, \quad t,s \in (0,1), \tag{B2}$$
$$z = (1-s)^{1/m}.$$

1. Volume of a superball

The volume of an object between the surface $z = f(x,y)$ and region A in the xy plane is given by

$$V = \iint_A f(x,y)\,dx\,dy, \tag{B3}$$

which for the case of the superball becomes

$$V = \iint_A \sqrt[m]{1 - x^m - y^m}\,dx\,dy. \tag{B4}$$

By substituting the x and y for the expressions given by the parametrization in Eq. (B2), we find

$$V = 8\int_0^1 \int_0^1 \sqrt[m]{1 - (t^{1/m}s^{1/m})^m - [(1-t)^{1/m}s^{1/m}]^m} \times J_{st}\,ds\,dt, \tag{B5}$$

where J_{st} is the Jacobian determinant needed when more than one variable is substituted

$$J_{st} = \begin{vmatrix} \frac{1}{m}t^{1/m-1}s^{1/m} & -\frac{1}{m}(1-t)^{1/m-1}s^{1/m} \\ \frac{1}{m}t^{1/m}s^{1/m-1} & \frac{1}{m}(1-t)^{1/m}s^{1/m-1} \end{vmatrix} = \frac{1}{m^2}(1-t)^{(1/m-1)}\,t^{(1/m-1)}\,s^{(2/m-1)}. \tag{B6}$$

For the volume of a superball, we then arrive at

$$V = 8\int_0^1 \int_0^1 \frac{1}{m^2}(1-t)^{(1/m-1)}t^{(1/m-1)}s^{(2/m-1)} \times (1-s)^{1/m}\,ds\,dt = \frac{8}{m^2}\int_0^1 s^{(2/m-1)}(1-s)^{1/m}\,ds \times \int_0^1 (1-t)^{(1/m-1)}t^{(1/m-1)}\,dt, \tag{B7}$$

in which we recognize the two integrals as Beta functions $B(x,y)$,

$$B(x,y) = \int_0^1 q^{(x-1)}(1-q)^{(y-1)}\,dq. \tag{B8}$$

Equation (B7) then transforms to

$$V = \frac{8}{m^2}B\left(\frac{2}{m}, \frac{1}{m}+1\right)B\left(\frac{1}{m}, \frac{1}{m}\right). \tag{B9}$$

Since for $B(x,y)$

$$B(x,y) = \frac{\Gamma(x)\Gamma(y)}{\Gamma(x+y)} \tag{B10}$$

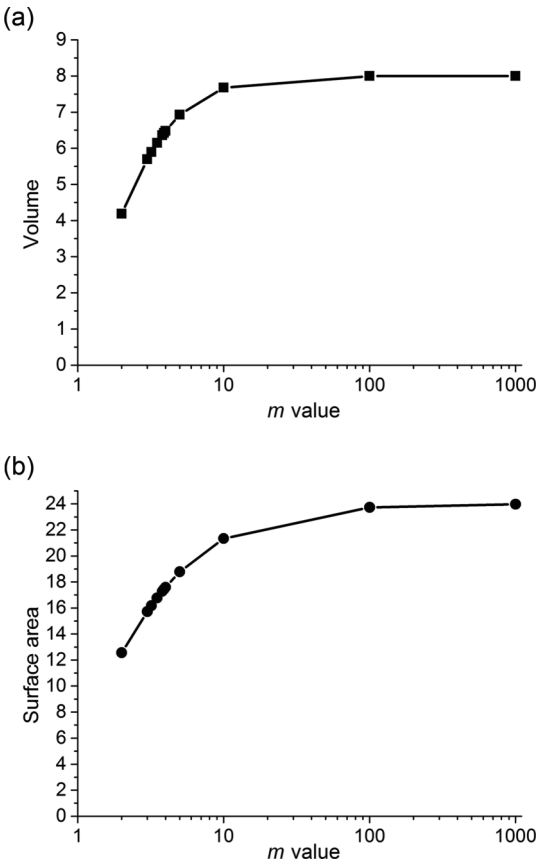

FIG. 11. Numerically calculated volume V and surface area S of a superball with $r = 1$ and increasing deformation parameter m. The analytically known cases are for $m = 2$ (sphere) and $m \to \infty$ (perfect cube).

holds, where Γ is the Gamma function, the volume of a superball is given by

$$V = \frac{8}{m^2}\frac{[\Gamma(1/m)]^2\Gamma(1/m+1)}{\Gamma(3/m+1)} = \frac{8}{3m^2}\frac{[\Gamma(1/m)]^3}{\Gamma(3/m)}. \tag{B11}$$

Figure 11(a) shows the volume of a superball with radius $r = 1$ ranging from $m = 2$ to 10^3 calculated numerically using Eq. (B11). At the extreme cases [$m = 2$ and 10^3 (approximately infinity)], the expected volumes of 4.2 [$(\frac{4}{3}\pi)^3$] and 8.0 [$(2)^3$] are found.

2. Surface area of a superball

To obtain an expression for the surface area of a superball, we again use the parametric representation of a superball with deformation parameter m and radius $r = 1$, given in Eq. (B2). The surface area of an object is defined as

$$S = \iint \|\vec{r}_s \times \vec{r}_t\|\,ds\,dt, \tag{B12}$$

with

$$\vec{r}_s = \frac{\partial x}{\partial s}\hat{\imath} + \frac{\partial y}{\partial s}\hat{\jmath} + \frac{\partial z}{\partial s}\hat{k}, \tag{B13a}$$

$$\vec{r}_t = \frac{\partial x}{\partial t}\hat{\imath} + \frac{\partial y}{\partial t}\hat{\jmath} + \frac{\partial z}{\partial t}\hat{k}. \tag{B13b}$$

In the case of a superball, this expression is

$$S = 8\int_0^1\int_0^1 \|\vec{r}_s \times \vec{r}_t\| ds\, dt, \tag{B14}$$

where the cross product is equal to

$$\begin{aligned}\vec{r}_s \times \vec{r}_t &= \begin{vmatrix} \hat{\imath} & \hat{\jmath} & \hat{k} \\ \frac{1}{m}t^{1/m}s^{(1/m-1)} & \frac{1}{m}(1-t)^{1/m}s^{(1/m-1)} & -\frac{1}{m}(1-s)^{(1/m-1)} \\ \frac{1}{m}t^{(1/m-1)}s^{1/m} & -\frac{1}{m}(1-t)^{(1/m-1)}s^{1/m} & 0 \end{vmatrix} \\ &= -\frac{1}{m^2}(1-s)^{(1/m-1)}(1-t)^{(1/m-1)}s^{1/m}\hat{\imath} + \frac{1}{m^2}(1-s)^{(1/m-1)}t^{(1/m-1)}s^{1/m}\hat{\jmath} \\ &\quad - \frac{1}{m^2}t^{(1/m-1)}(1-t)^{(1/m-1)}s^{(2/m-1)}\hat{k}. \end{aligned} \tag{B15}$$

The absolute value of this cross product then is

$$\begin{aligned}\|\vec{r}_s \times \vec{r}_t\| &= \sqrt{(i\hat{\imath})^2 + (j\hat{\jmath})^2 + (k\hat{k})^2} \\ &= \frac{1}{m^2}\sqrt{(1-s)^{(2/m-2)}(1-t)^{(2/m-2)}s^{2/m} + (1-s)^{(2/m-2)}t^{(2/m-2)}s^{2/m} + t^{(2/m-2)}(1-t)^{(2/m-2)}s^{(4/m-2)}}. \end{aligned} \tag{B16}$$

When we substitute Eq. (B16) in Eq. (B14), we find the expression for the surface area of a superball

$$S = 8\int_0^1\int_0^1 \frac{1}{m^2}\sqrt{(1-s)^{(2/m-2)}(1-t)^{(2/m-2)}s^{2/m} + (1-s)^{(2/m-2)}t^{(2/m-2)}s^{2/m} + t^{(2/m-2)}(1-t)^{(2/m-2)}s^{(4/m-2)}}ds\, dt. \tag{B17}$$

This equation can be evaluated analytically for $m = 2$, for the case of a sphere. Equation (B17) then reduces to $S = 4\pi$. For other values of m, the expression is evaluated numerically. As m approaches infinity, the shape of the superball approaches that of a perfect cube for which the surface area is $S = 24$. To confirm the correctness of this equation when evaluated numerically, we calculated the surface area of a superball with $r = 1$ for increasing values of m. The known extremes should then correspond to $S_{m=2} = 4\pi$ and $S_{m\to\infty} = 24$. Figure 11(b) shows the calculated surface area as a function of m, with $m = 10^3$ approximating infinity. It is clear that the calculated surface area for $m = 2$ is correct and that it grows to the expected value for high-m values, indicating that the calculated surface areas can reliably be used.

[1] J. Bear, *Dynamics of Fluids in Porous Media*, 1st ed. (Dover, New York, 1988).
[2] H. Verweij, Curr. Opin. Chem. Eng. **1**, 156 (2012).
[3] E. Guyon, L. Oger, and T. Plona, J. Phys. D **20**, 1637 (1987).
[4] H. Darcy, *Les Fontaines Publiques de la Ville de Dijon* (Dalmont, Paris, 1856).
[5] C. F. Berg, Transp. Porous Med. **103**, 381 (2014).
[6] S. Neuman, Acta Mech. **25**, 153 (1977).
[7] D. Thies-Weesie and A. Philipse, J. Colloid Interf. Sci. **162**, 470 (1994).
[8] A. Philipse and C. Pathmamanoharan, J. Colloid Interf. Sci. **159**, 96 (1993).
[9] R. Chapuis and M. Aubertin, *Predicting the Coefficient of Permeability of Soils Using the Kozeny-Carman Equation* (École Polytechnique de Montréal, Montreal, 2003).
[10] P. Xu and B. Yu, Adv. Water Resour. **31**, 74 (2008).
[11] P. Carman, Chem. Eng. Res. Des. **75**, S32 (1997).
[12] A. Burggraaf and L. Cot, *Fundamentals of Inorganic Membrane Science and Technology* (Elsevier, Amsterdam, 1996).
[13] B. Bettens, S. Dekeyzer, B. van der Bruggen, J. Degrève, and C. Vandecasteele, J. Phys. Chem. B **109**, 5216 (2005).
[14] H. Hsieh, R. Bhave, and H. Fleming, J. Membrane Sci. **39**, 221 (1988).
[15] A. Leenaars and A. Burggraaf, J. Colloid Interf. Sci. **105**, 27 (1985).
[16] I. Malinouskaya, V. V. Mourzenko, J.-F. Thovert, and P. M. Adler, Phys. Rev. E **80**, 011304 (2009).
[17] N. Chikhi, O. Coindreau, L. Li, W. Ma, V. Taivassalo, E. Takasuo, S. Leininger, R. Kulenovic, and E. Laurien, Ann. Nucl. Energy **74**, 24 (2014).
[18] A. Zick and G. Homsy, J. Fluid Mech. **115**, 13 (1982).
[19] D. Thies-Weesie, A. Philipse, and S. Kluijtmans, J. Colloid Interf. Sci. **174**, 211 (1995).
[20] L. Rossi, S. Sacanna, W. Irvine, P. Chaikin, D. Pine, and A. Philipse, Soft Matter **7**, 4139 (2011).
[21] S. Castillo, S. Ouhajji, S. Fokker, B. Erné, C. Schneijdenberg, D. Thies-Weesie, and A. Philipse, Microporous Mesoporous Mater. **195**, 75 (2014).

[22] J. Meijer, F. Hagemans, L. Rossi, D. Byelov, S. Castillo, A. Snigirev, I. Snigireva, A. Philipse, and A. Petukhov, Langmuir **28**, 7631 (2012).
[23] J. Meijer, D. Byelov, L. Rossi, A. Snigirev, I. Snigireva, A. Philipse, and A. Petukhov, Soft Matter **9**, 10729 (2013).
[24] H. Yang, S. He, H. Chen, and H. Tuan, Chem. Mater. **26**, 1785 (2014).
[25] G. Singh, H. Chan, A. Baskin, E. Gelman, N. Repnin, P. Kral, and R. Klajn, Science **345**, 1149 (2014).
[26] Y. Zhang, F. Lu, D. van der Lelie, and O. Gang, Phys. Rev. Lett. **107**, 135701 (2011).
[27] R. Ni, A. P. Gantapara, J. de Graaf, R. van Roij, and M. Dijkstra, Soft Matter **8**, 8826 (2012).
[28] Y. Jiao, F. H. Stillinger, and S. Torquato, Phys. Rev. E **81**, 041304 (2010).
[29] Y. Jiao, F. H. Stillinger, and S. Torquato, Phys. Rev. E **79**, 041309 (2009).
[30] R. D. Batten, F. H. Stillinger, and S. Torquato, Phys. Rev. E **81**, 061105 (2010).
[31] A. Donev, I. Cisse, D. Sachs, E. Variano, F. Stillinger, R. Connelly, S. Torquato, and P. Chaikin, Science **303**, 990 (2004).
[32] S. Sacanna, L. Rossi, A. Wouterse, and A. Philipse, J. Phys.: Condens. Matter **19**, 376108 (2007).
[33] K. Sing, Pure Appl. Chem. **54**, 2201 (1982).
[34] T. Sugimoto and K. Sakata, J. Colloid Interf. Sci. **152**, 587 (1992).
[35] L. Rossi, Colloidal superballs, Ph.D. thesis, Universiteit Utrecht, 2012.
[36] A. Philipse, B. Bonekamp, and H. Veringa, J. Am. Ceram. Soc. **73**, 2720 (1990).
[37] V. de Villeneuve, Structure and dynamics at colloidal boundaries, Ph.D. thesis, Utrecht University, 2008.
[38] J. Hilhorst, Defects in colloidal crystals, Ph.D. thesis, Utrecht University, 2012.
[39] J. Baker and A. Kudrolli, Phys. Rev. E **82**, 061304 (2010).
[40] S. Castillo, C. Pompe, J. van Mourik, D. Verbart, D. Thies-Weesie, P. de Jongh, and A. Philipse, J. Mater. Chem. A **2**, 10193 (2014).
[41] L. Durlofsky and J. Brady, Phys. Fluids **30**, 3329 (1987).
[42] D. Koch, R. Hill, and A. Sangani, Phys. Fluids **10**, 3035 (1998).